

A model with interaction of dark components and recent observational data

S. Pan^{1,*} and G. S. Sharov^{2,†}

¹*Department of Physical Sciences, Indian Institute of Science Education
and Research – Kolkata, Mohanpur- 741246, West Bengal, India*

²*Tver State University, 170002, Sadovyy per. 35, Tver, Russia*

In the proposed model with interaction between dark energy and dark matter, we consider cosmological scenarios with different equations of state (w_d) for dark energy. For both constant and variable equation of state, we analyze solutions for dark energy and matter in 7 variants of the model. We investigate exact analytic solutions for $w_d =$ constant equation of state, and several variants of the model for variable w_d . These scenarios are tested with the current astronomical data from Type Ia Supernovae, baryon acoustic oscillations and the Hubble parameter $H(z)$. Finally, we compare our interacting model with some known cosmological models.

PACS numbers: 98.80.-k, 95.35.+d, 95.36.+x, 98.80.Es.

1. INTRODUCTION

A dramatic change in the dynamic history of the universe happened since 1998 when observations from Type Ia Supernovae [1, 2] claimed our universe to be expanding with certain acceleration. This peculiar result was verified in several independent observations [3–7] supporting the present accelerating phase of our universe. However, this observational prediction required a perfect theoretical explanation behind such a scenario, and finally, the cosmologists came up to the conclusion that our universe must contain some exotic components with large negative pressure. In equation of state (hereafter we call it as EoS) of these components, the ratio of total pressure to the total energy density satisfies the condition “ $< -1/3$ ”. The components with this condition are dubbed “Dark Energy” to differ from other normal matter components (with positive pressure) in our universe. However, among the several dark energy candidates, the best description for our present accelerating universe is the Λ CDM model due to its satisfactory agreement with the current astronomical data we have. Still, the model suffers with two very known serious problems: the first one, known as the cosmological constant problem, is in huge (of the order 10^{121}) difference between the observed value of the cosmological constant and its predicted value by the quantum field theory [8]. The second problem, the cosmic coincidence problem [9], is in surprising fact, that the dark energy density has the same order of magnitude as the matter density in our universe today, though these two quantities have different laws of evolution.

On the other hand, observations [1–7] show that the accelerating phase is a late-time phenomenon, starting at a redshift $z \sim 1$. According to the hot big bang cosmology, before the present acceleration our universe went through a decelerating radiation and matter dominating phases. So, we have the main question at this point. Did

our universe contain some dark energy component which was insignificant during the phase of deceleration and now it began dominating over the matter sector? Two possible probable answers could be like this: may be the dark energy component is dynamical in nature, or, may be there is an energy exchange programme between dark matter and dark energy which, as a result, forces the dark energy component to accelerate our universe.

The case of dynamical dark energy has been widely studied in the literature (see the review [10] and the references therein) as an alternative explanation for Λ . Unfortunately, these models suffer from several unexplained problems. In particular, recent observations [11–15] claim that the EoS for the dark energy w is slightly more negative than the cosmological constant, i.e., $w < -1$. In order to describe this stage, we need some phantom scalar field which violates the dominant energy condition $p_\phi + \rho_\phi > 0$, and the energy density (ρ_ϕ), pressure (p_ϕ) assume the forms $\rho_\phi = -\frac{1}{2}\dot{\phi}^2 + V(\phi)$, $p_\phi = -\frac{1}{2}\dot{\phi}^2 - V(\phi)$, leading to $\omega_\phi < -1$. But, it differs from the normal scale field from the wrong sign in the kinetic term [16]. Although the phantom scalar field is a promising candidate for describing the $w < -1$ phase, but, at the classical and quantum levels, the scalar field solutions suffer from instabilities [17, 18]. Further, the models have some serious theoretical problems [19–21].

On the other hand, the interacting dynamics is quite interesting and useful. The dynamics of the universe gets richer while we bring the interaction between the dark sectors, however, we get back the non-interacting scenario when we make this interaction to be ‘zero’. However, the interacting dynamics became popular since this mechanism was found to alleviate the cosmic coincidence problem [22–35] (for a review on interacting dark energy see Refs. [36, 37]). Further, it has been discussed that some appropriate choice of an interaction between the dark components can influence effectively on the perturbation analysis which results in quite notable differences in the lowest multipoles of the cosmic microwave background spectrum [38, 39]. Moreover, the realization of a phantom universe through interacting dynamics, as sug-

*Electronic address: span@iiserkol.ac.in

†Electronic address: german.sharov@mail.ru

gested in [40, 41], has been slightly favored by the current observational data [42]. Thus, based on the above arguments, it is evident that one can not exclude the possibility of mutual interaction among the dark sectors, and this can be considered as an alternative description for our present universe.

In the present work we consider dark energy (DE) and the cold dark matter (CDM) to be the dominant sources in our universe, which are interacting in nature. For our analysis we use the general analytic form [43] of this interaction, which is the linear combination of DE and matter energy densities. Then we constrain model parameters by the joint analysis of Union 2.1, Hubble and baryon acoustic oscillation (BAO) data sets. It is worth noting that the present model with interacting dark components works well in comparison with the Λ CDM model and other popular cosmological models (Sect. 5).

The paper is organized as follows: In section 2, we describe the basic equations of interacting dynamics in the non-flat FLRW model. For the linear interaction between DE and CDM, section 3 presents the analytic solutions for $w_d = \text{const}$, in the EoS of DE and 5 variants of the model for variable w_d . In section 4, we shortly discuss different joint data analysis techniques and the results of their application to the considered several variants of our model. In section 5, we compare this model with other popular models in describing the same observational data. Finally, in section 6, we summarize the results of the work.

2. INTERACTING DYNAMICS IN FLRW UNIVERSE

On the largest scale, our universe is homogeneous and isotropic in nature, its geometry is described by the Friedmann-Lemaître-Robertson-Walker (FLRW) line element

$$ds^2 = -dt^2 + a^2(t) \left[\frac{dr^2}{1 - kr^2} + r^2(d\theta^2 + \sin^2\theta d\phi^2) \right], \quad (1)$$

where $a(t)$ (hereafter we shall denote it by ‘ a ’) is the scale factor of the universe, k is the curvature sign of the space-time, which for open, flat and closed universe takes the values $-1, 0, +1$, respectively. The description for the matter sector in our universe in agreement with the homogeneous and isotropic FLRW metric assumes a perfect fluid distribution with the energy-momentum tensor

$$T_{\mu\nu} = (p + \rho)u_\mu u_\nu + pg_{\mu\nu}, \quad (2)$$

where p, ρ are respectively the pressure and the energy density of a perfect fluid under consideration, u_μ is the four velocity of a fluid particle.

Now, the governing dynamical equations of our universe are obtained by solving the Einstein’s field equa-

tions without cosmological constant

$$G_{\mu\nu} = 8\pi G T_{\mu\nu},$$

which for the metric (1) and the energy-momentum tensor of the perfect fluid (2) lead to the following well known Friedmann equations:

$$H^2 + \frac{k}{a^2} = \frac{8\pi G}{3}\rho, \quad (3)$$

$$\frac{\ddot{a}}{a} = -\frac{4\pi G}{3}(3p + \rho), \quad (4)$$

where $H = \dot{a}/a$ is the Hubble parameter, $8\pi G$ is the Einstein’s gravitational constant. From the Bianchi’s identity we get the conservation equation $T_{\nu;\mu}^\mu = 0$, that for the perfect fluid takes the form

$$\dot{\rho} + 3\frac{\dot{a}}{a}(p + \rho) = 0. \quad (5)$$

The last equation (5) could also be obtained by using Eqs. (3) and (4). However, we have two independent equations, which in principle can describe the complete dynamics of the universe.

Now, it is clear that under barotropic equation of state (EoS) $p = w\rho$, where $w = \text{const}$, is the EoS parameter for the perfect fluid, the conservation equation (5) can be solved as $\rho = \rho_0 a^{-3(1+w)}$, ρ_0 being the present value of the energy density. We note that for the present value of the scale factor here and below we suppose $a(t_0) = a_0 = 1$ (t_0 is the present value of the cosmic time). So, if we suppose that the cold matter with $p = 0$ satisfies Eq. (5) separately (in other words, it does not interact with dark energy), we have $\rho_m = \rho_{m0} a^{-3}$. If we consider an independent dark energy component with EoS $w_d = \text{const}$, we have $\rho_d = \rho_{d0} a^{-3(1+w_d)}$. Here ρ_{m0}, ρ_{d0} are the present day values of the densities for cold matter and the dark energy, respectively.

According to the present day observations [12], most of the universe content is unknown to us. Around 26% of the total energy budget is filled with pressureless cold dark matter, 70% in the form of dark energy (DE), rest are filled with about 4% of baryons and negligible radiation (0.005%). So, the present universe is completely dominated by the cold dark matter and dark energy with energy densities ρ_{dm} and $\rho_{de} \equiv \rho_d$ respectively. We introduce an interacting scenario between cold dark matter (CDM) and DE through an phenomenological interaction term Q which in general could be $Q = Q(H, \rho_{dm}, \rho_d)$. Therefore, the introduction of Q modify the conservation equations for CDM and DE as

$$\dot{\rho}_{dm} + 3H\rho_{dm} = Q, \quad (6)$$

$$\dot{\rho}_d + 3H(1 + w_d)\rho_d = -Q, \quad (7)$$

whereas for the total energy density of CDM and DE $\rho_T = \rho_m + \rho_d$ the energy conservation satisfies Eq. (5)

$$\dot{\rho}_T + 3\frac{\dot{a}}{a}(\rho_T + p_T) = 0, \quad (8)$$

which is the sum of Eqs. (6) and (7). The total density ρ in Eqs. (3)–(5) includes the density ρ_T of CDM and DE and the baryon contribution ρ_b : $\rho = \rho_T + \rho_b$ (here and below we neglect radiation). Baryons do not interact with DE in Eqs. (6), (7), their density $\rho_b = \rho_m - \rho_{dm}$ satisfies the same equation (5) or (8).

However, using Eq. (8), one can express ρ_d and ρ_{dm} as follows:

$$\rho_d = -\frac{\rho_T + \rho'_T}{w_d}, \quad (9)$$

$$\rho_{dm} = \frac{\rho'_T + (1 + w_d)\rho_T}{w_d}. \quad (10)$$

Here primes denote derivatives with respect to $x = 3 \ln a$. So, once ρ_T is determined, the evolution equations for cold dark matter and dark energy can be completely understood. The interaction term Q in Eqs. (6), (7) is phenomenological in nature, however, we will concentrate mostly on such interactions, which either provide analytic solutions for the components or successfully describe the current observational data.

3. VARIANTS OF THE MODEL

We introduce the following interaction [30, 43]

$$Q = 3\lambda_m H \rho_{dm} + 3\lambda_d H \rho_d, \quad (11)$$

where λ_m, λ_d are the coupling parameters. Due to the expression (11) the conservation equations (6) and (7) are modified, and finally, we get the following second order differential equation:

$$\begin{aligned} \rho''_T + \left(2 + w_d + \lambda_d - \lambda_m - \frac{w'_d}{w_d}\right) \rho'_T \\ + \left[(1 + w_d)(1 - \lambda_m) + \lambda_d - \frac{w'_d}{w_d}\right] \rho_T = 0. \end{aligned} \quad (12)$$

Now, until the nature of the DE equation of state be discovered, it is really difficult to infer about evolution of dark energy as well as dark matter. Still, we can look for possible evolution equations if w_d in Eq. (12) is constant or variable, and finally, we aim to study them from recent observational data.

3.1. The case for constant w_d in DE EoS

If $w_d = \text{const}$, the solution of the differential equation (12) becomes [33]

$$\rho_T = \rho_1 a^{3m_+} + \rho_2 a^{3m_-}, \quad (13)$$

where ρ_1, ρ_2 are integration constants, m_+, m_- are

$$m_{\pm} = \frac{\lambda_m - w_d - \lambda_d - 2 \pm \sqrt{(\lambda_m + w_d + \lambda_d)^2 - 4\lambda_m \lambda_d}}{2}.$$

Now, using (13), we have the explicit analytic solutions for dust and dark energy as follows:

$$\begin{aligned} \rho_{dm} &= \rho_1 \frac{w_d + 1 + m_+}{w_d} a^{3m_+} + \rho_2 \frac{w_d + 1 + m_-}{w_d} a^{3m_-}, \\ \rho_d &= -\frac{\rho_1(1 + m_+) a^{3m_+} + \rho_2(1 + m_-) a^{3m_-}}{w_d}. \end{aligned}$$

We note that there are very few works in the literature, where the analytic solutions for interacting dark energy has been explicitly found [33, 43]¹. Thus, the analytic solutions for the present interaction is one of the interesting findings in the literature of interacting dynamics.

However, we note that in Ref. [43] the authors found the analytic solutions for this linear interaction in a restricted way, i.e. they excluded the product $\lambda_m \lambda_d$ and analyzed the solutions for $m_+ = -(1 - \lambda_m)$, $m_- = -(1 + \lambda_d + w_d)$, which means that complete information was not reported. Also, the analysis of this model was performed only by 194 Supernovae Type Ia data from [45, 46] where the nature of the coupling parameters and their estimations were not addressed. Thus, in comparison with the previous study, the present one has two fold importance: (i) the solutions (13) for general (m_+, m_-) completes the study without any information loss, and (ii) here we employ the current observational data which provide better observational constraints on all model parameters. Thus, under (i) and (ii), the present analytic interacting dark energy model could produce some interesting information about this interacting dark energy-dark matter model while constraining it by recent observational data sets.

Further, the present day density parameters for dark matter ($\equiv \Omega_{dm0}$) and dark energy ($\equiv \Omega_{d0}$) in terms of the density parameters for the equivalent two fluids Ω_1 and Ω_2 are given by

$$\Omega_{dm0} = \Omega_1 \frac{w_d + 1 + m_+}{w_d} + \Omega_2 \frac{w_d + 1 + m_-}{w_d}, \quad (14)$$

$$\Omega_{d0} = -\frac{\Omega_1(1 + m_+) + \Omega_2(1 + m_-)}{w_d}, \quad (15)$$

where $\Omega_i = 8\pi G \rho_i / 3H_0^2$. The values Ω_1, Ω_2 can be expressed by using the above two equations (14), (15), their consequence $\Omega_{dm0} + \Omega_{d0} = \Omega_1 + \Omega_2$ and the equality

$$\Omega_{dm0} + \Omega_{d0} + \Omega_{b0} + \Omega_k = \Omega_1 + \Omega_2 + \Omega_{b0} + \Omega_k = 1,$$

results in from Eq. (3) at the present time $t = t_0$. Here $\Omega_{b0} = \Omega_b(t_0)$, $\Omega_k = -k/(a_0 H_0)^2$. In particular,

$$\Omega_1 = \frac{w_d \Omega_{dm0} - (1 + w_d + m_-)(1 - \Omega_{b0} - \Omega_k)}{m_+ - m_-}. \quad (16)$$

Also, we note that the present value of the total density parameter for matter is $\Omega_{m0} = \Omega_{dm0} + \Omega_{b0}$. In Sect. 4

¹ Analytic solutions with two interacting scalar fields may be found in Ref. [44]

(see Fig. 1) we investigate how solutions (13) describe the observational data for Type Ia supernovae, baryon acoustic oscillations and for the Hubble parameter $H(z)$.

3.2. Variable w_d in DE EoS

The nature of dark energy is still elusive, after completion of several dark energy projects. Observations support models with various forms of DE resulting in effective value of $w = p/\rho$ close to ‘-1’ [11, 12]. They include not only Λ CDM with well known advantages and vague nature of Λ , but also models with different EoS for some DE component.

Since no one has a concrete answer to the question about nature of DE, thus, one may, of course, think of the most suitable EoS for DE, keeping in mind that it is really difficult to find some ‘at least’ approximate form for w_d which could survive with the present observational data. So, while choosing some variable form for EoS, we need to solve Eq. (12) and consequently, we must be very cautious in order to see its effect on our universe.

There are several interacting dark energy models with possibility of variable EoS in DE, where reasonable attention has been paid to observational data. In Ref. [47], the authors investigated an interacting scenario for $Q = 3H\lambda_m\rho_m$ with Chevallier-Polarski-Linder (CPL) parametrization [48, 49] as the equation of state in DE. Also, in Ref. [29] the authors studied the present linear interaction (11) with CPL parametrization but with very old data (182 Gold Type Ia Supernovae data [50]). Thus, considering the linear interaction (11) in our discussion, we aim to investigate the interacting dynamics between CDM and DE with some new variable equations of state in w_d including CPL [48, 49] and linear parametrization [51–53] by Union 2.1 compilation [54] along with Hubble parameter measurements and baryon acoustic oscillation data.

Let us first begin our analysis with the following generalized ansatz

$$\frac{w'_d}{w_d} = \alpha w_d + \beta, \quad (17)$$

where α, β are real numbers. The solution of Eq. (17) is

$$w_d = \left[\left(\frac{1}{w_{d0}} + \frac{\alpha}{\beta} \right) a^{-3\beta} - \frac{\alpha}{\beta} \right]^{-1}, \quad (18)$$

where w_{d0} is the present value of w_d . In particular, we consider the following partial cases

$$\text{Ansatz I: } \alpha = 0, \quad w_d = w_{d0}a^{3\beta}; \quad (19)$$

$$\text{Ansatz II: } \beta = 0, \quad w_d = w_{d0}/(1 - \alpha w_{d0}x), \quad (20)$$

We also consider separately the following ansatz:

$$\text{Ansatz III: } \alpha = 1, \quad (21)$$

which is attractive, because in this case under the condition $\lambda_m = 0$ coefficients of equation (12) become constant, and its general solution has the simple form [43]

$$\rho_T = \tilde{\rho}_1 a^{-3} + \tilde{\rho}_2 a^{3(n-1)}, \quad (22)$$

where $n = \beta - \lambda_d = \text{const}$, and $\tilde{\rho}_1 > 0$, $\tilde{\rho}_2 > 0$ are integration constants.

It is interesting to consider the model with interaction (11) and Chevallier-Polarski-Linder (CPL) parametrization [48, 49]

$$\text{Ansatz IV: } w_d(z) = w_{d0} + w_1 \frac{z}{1+z}, \quad (23)$$

and also with linear parametrization [51–53]

$$\text{Ansatz V: } w_d(z) = w_{d0} + w_1 z. \quad (24)$$

Here w_{d0}, w_1 are two free parameters to be constrained by the observational data in which w_{d0} is the present value of w_d as mentioned earlier. The dependencies of $w_d(z)$ in (23) and (24) are alternative to (18).

4. JOINT ANALYSIS

In order to analyze our model with recent observational data, we use $N_{SN} = 580$ data points from Union 2.1 [54], $N_H = 39$ observed Hubble data points [55–70] and $N_{BAO} = 17$ baryon acoustic oscillation data [61–79]. For each data sets, we can have χ^2_i ($i = SN, H, BAO$) for Union 2.1, Hubble data and BAO data set respectively, and as χ^2_i for all i are Gaussian in nature, so we can add the χ^2 's for the three data sets. Finally, we can find the total χ^2_Σ for the model by summing all the χ^2_i 's as follows

$$\chi^2_\Sigma = \chi^2_{SN} + \chi^2_H + \chi^2_{BAO}, \quad (25)$$

By minimizing this χ^2_Σ , we will obtain the best fit values of the model parameters. In the next subsections, we shortly describe different data sets and their χ^2 tests.

4.1. Union 2.1 data points

Type Ia Supernovae are the first indication for existence of some dark energy in our universe [1, 2]. The observable quantities from a Type Ia supernova (SN Ia) are its redshift z and its apparent magnitude m_{obs} , but in the survey [54] values m_{obs} are recalculated into distance modulus

$$\mu_{obs} = m_{obs}(z) - M + \bar{\alpha}x_1 - \bar{\beta}c + \bar{\delta}P. \quad (26)$$

Here, additive terms include the SN Ia absolute magnitude M and corrections connected with deviations from mean values of lightcurve shape (x_1), SN Ia color (c) and mass of a host galaxy (the factor P). The parameters $M, \bar{\alpha}, \bar{\beta}$ and $\bar{\delta}$ are considered in Ref. [54] as nuisance parameters, and they are fitted simultaneously with H_0 and

other cosmological parameters in the flat Λ CDM model. This approach is usual in SN Ia analysis [80–82]. So values (26) in Ref. [54] may have a model dependent additive term (a systematic error) with concealed dependence on H_0 and other model parameters.

We have to keep in mind this fact, when we compare observable values (26) from Ref. [54] with theoretical values of distance modulus, corresponding to redshift z

$$\mu_{th}(z) = 5 \log_{10} \left(\frac{D_L(z)}{10 \text{pc}} \right) = 5 \log_{10} \frac{H_0 D_L}{c} + \mu_0. \quad (27)$$

Here $\mu_0 = 42.384 - 5 \log_{10} h$, $D_L(z)$ is the luminosity distance [1, 80]

$$D_L(z) = \frac{c(1+z)}{H_0} S_k \left(H_0 \int_0^z \frac{d\tilde{z}}{H(\tilde{z})} \right) \quad (28)$$

with

$$S_k(x) = \begin{cases} \sinh(x\sqrt{\Omega_k})/\sqrt{\Omega_k}, & \Omega_k > 0, \\ x, & \Omega_k = 0, \\ \sin(x\sqrt{|\Omega_k|})/\sqrt{|\Omega_k|}, & \Omega_k < 0. \end{cases}$$

The value $H_0 D_L/c$ in Eq. (27) is the Hubble free luminosity distance (for the majority of cosmological models) and only the term μ_0 [80] depend on the Hubble constant H_0 or $h = H_0/100 \text{ km s}^{-1} \text{Mpc}^{-1}$.

For any cosmological model, we fix its model parameters $\theta_1, \theta_2, \dots$, calculate functions $a(t)$, $z = a^{-1} - 1$, $H(z)$, the integral (28), and hence this model predicts theoretical values D_L^{th} or μ_{th} for the modulus (27). To compare these theoretical values with the observational data z_i and $\mu_{obs}(z_i)$ [54] we use the 580×580 covariance matrix C_{SN} from Ref. [54] and the function

$$\tilde{\chi}_{SN}^2(\theta_1, \dots) = \sum_{i,j=1}^{N_{SN}} \Delta\mu_i (C_{SN}^{-1})_{ij} \Delta\mu_j, \quad (29)$$

where $\Delta\mu_i = \mu_{th}(z_i, \theta_1, \dots) - \mu_{obs}(z_i)$.

To exclude the possible systematic errors in μ_{obs} mentioned above, we follow the marginalization procedure, suggested in Ref. [80], and consider below the minimum of the sum (29) over H_0 (or over μ_0)

$$\chi_{SN}^2 = \min_{\mu_0} \tilde{\chi}_{SN}^2 = \tilde{\chi}_{SN}^2 \Big|_{\mu_0=0} - \frac{B^2}{C}, \quad (30)$$

$$B = \sum_{i,j=1}^{N_{SN}} (\Delta\mu_i - \mu_0) (C_{SN}^{-1})_{ij}, \quad C = \sum_{i,j=1}^{N_{SN}} (C_{SN}^{-1})_{ij}.$$

In this paper, for all models we use the marginalized function (30) to describe the SNe Ia data [54].

4.2. Hubble parameter data

The Hubble parameter H at some certain redshift z can be measured from differential ages of galaxies [55–

z	$H_{obs}(z)$	σ_H	Refs	z	$H_{obs}(z)$	σ_H	Refs
0.070	69	19.6	[58]	0.570	96.8	3.4	[67]
0.090	69	12	[55]	0.593	104	13	[57]
0.120	68.6	26.2	[58]	0.600	87.9	6.1	[62]
0.170	83	8	[55]	0.680	92	8	[57]
0.179	75	4	[57]	0.730	97.3	7.0	[62]
0.199	75	5	[57]	0.781	105	12	[57]
0.200	72.9	29.6	[58]	0.875	125	17	[57]
0.240	79.69	2.99	[61]	0.880	90	40	[56]
0.270	77	14	[55]	0.900	117	23	[55]
0.280	88.8	36.6	[58]	1.037	154	20	[57]
0.300	81.7	6.22	[68]	1.300	168	17	[55]
0.340	83.8	3.66	[61]	1.363	160	33.6	[59]
0.350	82.7	9.1	[64]	1.430	177	18	[55]
0.352	83	14	[57]	1.530	140	14	[55]
0.400	95	17	[55]	1.750	202	40	[55]
0.429	91.8	5.3	[60]	1.965	186.5	50.4	[59]
0.430	86.45	3.97	[61]	2.300	224	8.6	[63]
0.440	82.6	7.8	[62]	2.340	222	8.5	[70]
0.480	97	62	[56]	2.360	226	9.3	[69]
0.570	87.6	7.8	[65]				

TABLE I: Hubble parameter values H_{obs} in $\text{km s}^{-1} \text{Mpc}^{-1}$ at different redshifts z with corresponding errors σ_H .

60] with using the following formula:

$$H(z) = \frac{\dot{a}}{a} = -\frac{1}{1+z} \frac{dz}{dt},$$

In addition, estimations of $H(z)$ may be extracted from line-of-sight BAO data [61–70].

In this analysis we use $N_H = 39$ observed Hubble parameter values [55–70] in the range $0.070 \leq z \leq 2.36$, which are listed in Table (I). The corresponding χ_H^2 is defined as

$$\chi_H^2 = \sum_{i=1}^{N_H} \left[\frac{H_{obs}(z_i) - H_{th}(z_i, \theta_j)}{\sigma_{H,i}^2} \right]. \quad (31)$$

4.3. BAO data

Observational data, connected with baryon acoustic oscillations (BAO), include the distance [6]

$$D_V(z) = \left[\frac{cz D_L^2(z)}{(1+z)^2 H(z)} \right]^{1/3},$$

and two measured values

$$d_z(z) = \frac{r_s(z_d)}{D_V(z)}, \quad A(z) = \frac{H_0 \sqrt{\Omega_{m0}}}{cz} D_V(z). \quad (32)$$

Here $r_s(z_d)$ is sound horizon size at the end of the drag era z_d . In this paper we use the fitting formula from Ref. [83]

$$r_s(z_d) = \frac{55.154 \exp[72.3(\Omega_\nu h^2 + 0.0006)^2]}{(\Omega_{m0} h^2)^{0.25351} (\Omega_{b0} h^2)^{0.12807}} \text{ Mpc.} \quad (33)$$

Here dependence on neutrino contribution Ω_ν is negligible for reasonable values $\sum m_\nu \leq 0.23 \text{ eV}$ [12] (below we suppose $\sum m_\nu = 0.06 \text{ eV}$ [12, 83]).

Calculations with similar observational data and with the function (33) were made in Ref. [84] for the models: Λ CDM, with generalized and modified Chaplygin gas and with quadratic equation of state (described below in Sect. 5). The best fitting value of Ω_{b0} in Eq. (33)

$$\Omega_{b0} = 0.044 \quad (34)$$

was obtained for the Λ CDM and appeared to be just the same for 3 other models in Ref. [84]. One should note that the value (34) is connected with the formula (33). Calculations in Ref. [84] with the more simple fitting formula $r_d = (r_d h)_{fid} \cdot h^{-1}$ for all 4 models demonstrated similar estimations of model parameters, but very weak dependence of them on Ω_{b0} . It is connected with similarity in properties of dark matter and baryons. Due to this reason we do not consider Ω_{b0} as a free model parameter and fix it in the form (34) for all models in this paper. The additional reason is necessity to minimize a number of free model parameters for considered scenarios.

To take into account all available BAO data [61–78] for parameters (32), we consider in this paper $N_B = 17$ data points for $d_z(z)$ and 7 data points for $A(z)$ presented in the Table II.

z	$d_z(z)$	σ_d	$A(z)$	σ_A	Refs	Survey
0.106	0.336	0.015	0.526	0.028	[73, 79]	6dFGS
0.15	0.2232	0.0084	-	-	[78]	SDSS DR7
0.20	0.1905	0.0061	0.488	0.016	[71, 74]	SDSS DR7
0.275	0.1390	0.0037	-	-	[71]	SDSS DR7
0.278	0.1394	0.0049	-	-	[72]	SDSS DR7
0.314	0.1239	0.0033	-	-	[74]	SDSS LRG
0.32	0.1181	0.0026	-	-	[67]	BOSS DR11
0.35	0.1097	0.0036	0.484	0.016	[71, 74]	SDSS DR7
0.35	0.1126	0.0022	-	-	[75]	SDSS DR7
0.35	0.1161	0.0146	-	-	[64]	SDSS DR7
0.44	0.0916	0.0071	0.474	0.034	[74]	WiggleZ
0.57	0.0739	0.0043	0.436	0.017	[65]	SDSS DR9
0.57	0.0726	0.0014	-	-	[67]	SDSS DR11
0.60	0.0726	0.0034	0.442	0.020	[74]	WiggleZ
0.73	0.0592	0.0032	0.424	0.021	[74]	WiggleZ
2.34	0.0320	0.0021	-	-	[70]	BOSS DR11
2.36	0.0329	0.0017	-	-	[69]	BOSS DR11

TABLE II: Values of $d_z(z) = r_s(z_d)/D_V(z)$ and $A(z)$ (32) with errors and references

Measurements of $d_z(z)$ and $A(z)$ from Refs. [71, 74] in Table II are not independent. So the χ^2 function for the values (32) is

$$\chi_{BAO}^2(\theta_j) = (\Delta d)^T C_d^{-1} \Delta d + (\Delta A)^T C_A^{-1} \Delta A, \quad (35)$$

where $\Delta d = d_z(z_i) - d_z^{th}$, $\Delta A = A(z_i) - A^{th}$. The elements of covariance matrices $C_d^{-1} = ||c_{ij}^d||$, $C_A^{-1} = ||c_{ij}^A||$ in Eq. (35) are [71, 74, 79]:

$$\begin{aligned} c_{33}^d &= 30124, & c_{38}^d &= -17227, & c_{88}^d &= 86977, \\ c_{1111}^d &= 24532.1, & c_{1114}^d &= -25137.7, & c_{1115}^d &= 12099.1, \\ c_{1414}^d &= 134598.4, & c_{1415}^d &= -64783.9, & c_{1515}^d &= 128837.6; \\ c_{1111}^A &= 1040.3, & c_{1114}^A &= -807.5, & c_{1115}^A &= 336.8, \\ c_{1414}^A &= 3720.3, & c_{1415}^A &= -1551.9, & c_{1515}^A &= 2914.9. \end{aligned}$$

Here $c_{ij} = c_{ji}$, the remaining matrix elements are $c_{ij} = 0$, if $i \neq j$, and $c_{ii} = 1/\sigma_i^2$.

4.4. Results, joint analysis for $w_d = \text{const}$

We investigated, how the χ^2 functions in Eqs. (29), (31), (35) and their sum (25) depend on model parameters for different variants of the model, considered in Sect. 3. For the model with $w_d = \text{const}$ and solution (13), the results of calculations are presented in Fig. 1. The top panels illustrate how the minimum of the sum (25) $\min \chi_\Sigma^2$ depend on one chosen parameter: H_0 , Ω_{m0} , λ_m , λ_d and Ω_k . Here we compare two cases: for the model with 6 free parameters including $\Omega_k \neq 0$ these dependencies are shown as blue thick lines, but for the flat case $\Omega_k = 0$ the corresponding graphs are red dashed lines.

In particular, in the top-left panel for the case $\Omega_k \neq 0$ the function $\min \chi_\Sigma^2(H_0)$ means $\min_{\Omega_{m0}, \Omega_k, w_d, \lambda_m, \lambda_d} \chi_\Sigma^2$. This blue curve essentially differs from the red dashed line, describing the flat case $\Omega_k = 0$. The values of absolute minima of χ_Σ^2 for these cases are presented below in Table III with optimal values and 1σ errors for model parameters. For example, for the Hubble constant we estimate $H_0 = 69.68^{+1.80}_{-1.75} \text{ km (s Mpc)}^{-1}$ for the flat case and $H_0 = 70.40^{+2.18}_{-2.13} \text{ km (s Mpc)}^{-1}$ for $\Omega_k \neq 0$; 1σ errors are extracted from the one-dimensional likelihood function $\mathcal{L}_\Sigma(H_0) \sim \exp(-\chi_\Sigma^2/2)$.

The similar estimation for Ω_{m0} is determined by the function $\min \chi_\Sigma^2(\Omega_{m0}) = \min_{H_0, \Omega_k, w_d, \lambda_m, \lambda_d} \chi_\Sigma^2$, if $\Omega_k \neq 0$. These graphs for $\Omega_k = 0$ and $\Omega_k \neq 0$ are rather close and have distinct minimum with small 1σ deviation $\Delta\Omega_{m0} \simeq 0.013$. It is connected with the factor $\sqrt{\Omega_{m0}}$ in the value $A(z)$ (32), so the contribution χ_{BAO}^2 in the sum (25) is very sensitive to Ω_{m0} values. Dependencies of $\min \chi_\Sigma^2$ on λ_m and λ_d in the top-right panels of Fig. 1 are asymmetric and not so sharp, they result in the estimations of λ_m , λ_d in Table III. In the top-right panel the dependence of $\min \chi_\Sigma^2$ on Ω_k yields the 1σ interval $\Omega_k = -0.124^{+0.213}_{-0.190}$, it includes values $\Omega_k \simeq 0$.

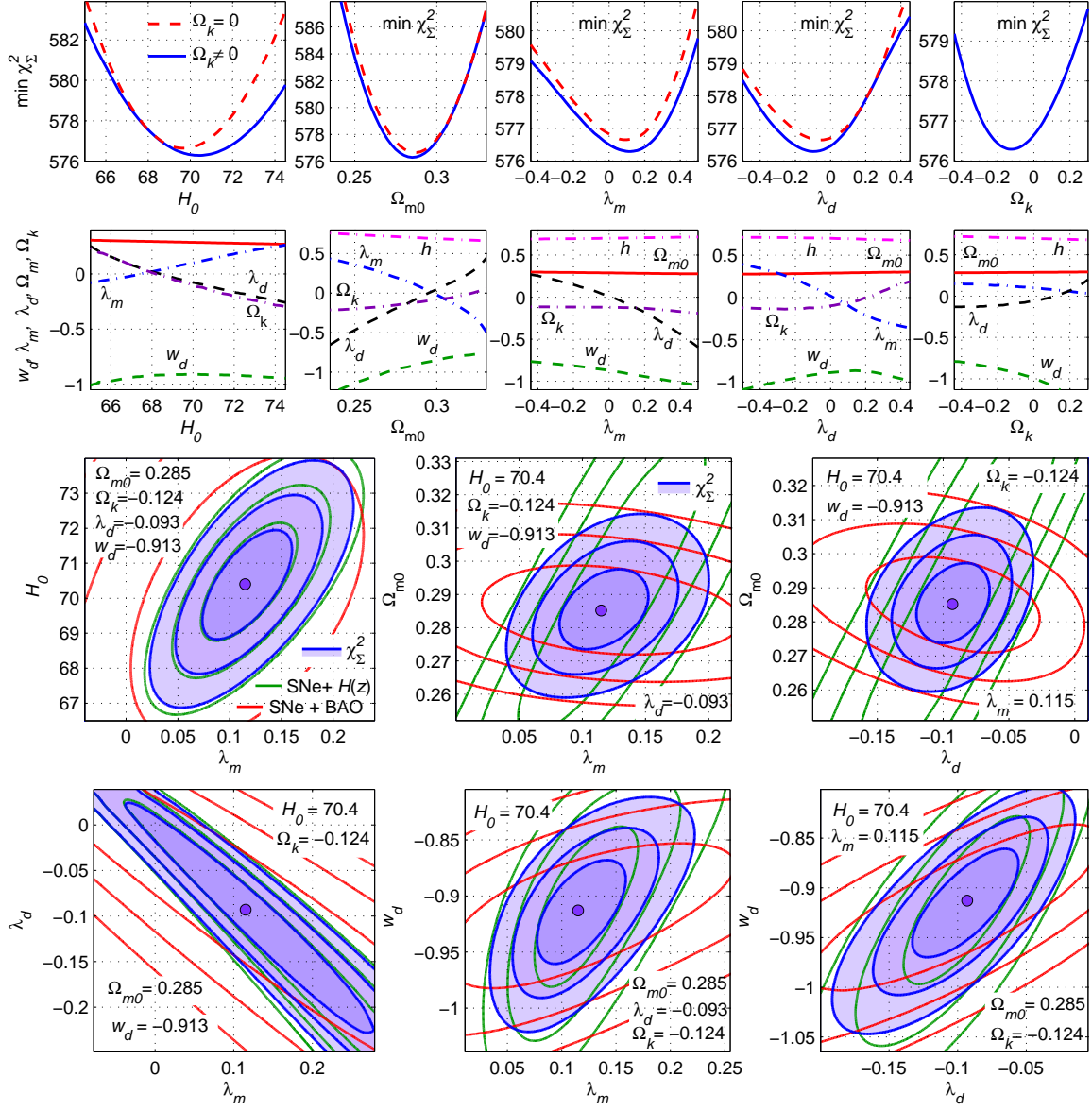


FIG. 1: For the model (11) with $w_d = \text{const}$ in the top panels we present dependence of $\min \chi_\Sigma^2$ on H_0 , Ω_{m0} , λ_m , λ_d and Ω_k for $\Omega_k \neq 0$ (blue solid lines) in comparison with the flat case $\Omega_k = 0$ (red dashed lines). The second row of panels shows how parameters of a minimum point depend on H_0 , Ω_{m0} , \dots , Ω_k . In other panels level lines in planes of 2 parameters are drawn at 1σ , 2σ and 3σ for χ_{SN}^2 (black), for $\chi_{SN}^2 + \chi_{BAO}^2$ (red), for $\chi_{SN}^2 + \chi_H^2$ (green) and for the sum χ_Σ^2 (filled contours); values of other parameters are fixed and shown.

The second row panels of Fig. 1 correspond to panels in the top line and present dependencies of coordinates of minima points (optimal values of parameters) on H_0, \dots, Ω_k for the function χ_Σ^2 if $\Omega_k \neq 0$. One can see that optimal values of λ_m and λ_d have distinct negative correlation (observed explicitly in the bottom-left panel), optimal values of Ω_{m0} and $h = H_0/100$ depend on other parameters rather weakly.

In 6 bottom panels of Fig. 1 we present the results of calculations as 1σ (68.27%), 2σ (95.45%) and 3σ (99.73%) level lines for the functions $\chi^2(p_1, p_2)$ in planes

of two parameters, if $\Omega_k = -0.124$ and other three parameters are fixed with their optimal values. These values are shown in the panels and tabulated in Table III. The mentioned level lines are shown for the $\chi_{SN}^2 + \chi_{BAO}^2$ function (red curves), for $\chi_{SN}^2 + \chi_H^2$ (green curves) and for the sum χ_Σ^2 as filled contours. Violet circles mark minimum points of χ_Σ^2 .

4.5. Results for $w_d \neq \text{const}$

In Sect. 3.2 we considered more general EoS for dark energy with variable w_d satisfying Eq. (17). This general ansatz with its solution (18) gives not only new possibilities, but also additional problems of the following two types: (i) two extra model parameters (3 parameters w_{d0} , α and β instead of one w_d); (ii) singularities in the past, which appear in different scenarios of the class (18).

These singularities connected with bad behavior of densities ρ_{dm} , ρ_d or their sum ρ_T at a moment t_s in the past, when the scale factor remains finite and nonzero ($a(t_s) \neq 0$), they may be classified into the following three types:

- a) $\lim_{t \rightarrow t_s} \rho_T = \infty$;
 - b) $\rho_{dm} < 0$, if $t < t_s$;
 - c) $\rho_d < 0$, if $t < t_s$.
- (36)

These cases resemble classification of singularities in Ref. [85]. For singularities (36) of the type (c) DE pressure $p_d(t_s)$ remains finite at the moment t_s , whereas $\rho_d(t_s) = 0$; they may be also divided into class (c1) with $p_d(t_s) = 0$ and finite $w_d = p_d/\rho_d$ and class (c2) with $p_d(t_s) \neq 0$, where w_d tends to infinity if $t \rightarrow t_s$. Possible singularities (36) compel us to be especially careful, when we calculate numerically parameters of effective scenarios in this model. We should exclude domains in parameter space with singular behavior of physical densities irrespective of type (36). The example of singular solution with type (c1) singularity (36) is shown in the bottom-left panel of Fig. 2.

We mentioned above, that the number N_p of model parameters for scenarios with variable w_d satisfying Eq. (17) is too large, it is disadvantage in competition with other models in accordance with information criteria [86–88]. So we have to exclude non-flat scenarios and fix in this section $\Omega_k = 0$. But even for the flat case we have $N_p = 7$ parameters: H_0 , Ω_{m0} , λ_m , λ_d , w_{d0} , α , β .

An attempt to exclude λ_m appeared to be unsuccessful: though in the case $\lambda_m = 0$, we can avoid some singularities (36) and instabilities in perturbations [89, 90], but the best value of the function (25) $\min \chi_\Sigma^2 \simeq 576.74$ is worth, than in the case $w_d = \text{const}$ (13) (but $\lambda_m \neq 0$). So we have to fix other parameters. First, we consider the case $\alpha = 0$ (19), denoted in Sect. 3.2 as Ansatz I.

For Ansatz I ($\alpha = 0$) we have no acceptable analytic solution of Eq. (12), so we investigate numerical solutions of the system (3), (6), (7), (11), (19) with natural initial conditions $\rho_m|_{t=t_0} = \rho_{m0}$, $\rho_d|_{t=t_0} = \rho_{d0}$ at the present day and integration “into the past”. For Ansatz I we can reach the best value $\min \chi_\Sigma^2 \simeq 576.29$, this solution is presented in Fig. 2 (in the top-left, top-right and bottom-right panels), and corresponding values of model parameters are tabulated in the “Ansatz I” line of Table III.

In the left panels of Fig. 2 we compare the regular solution with parameters from Table III (the top-left panel)

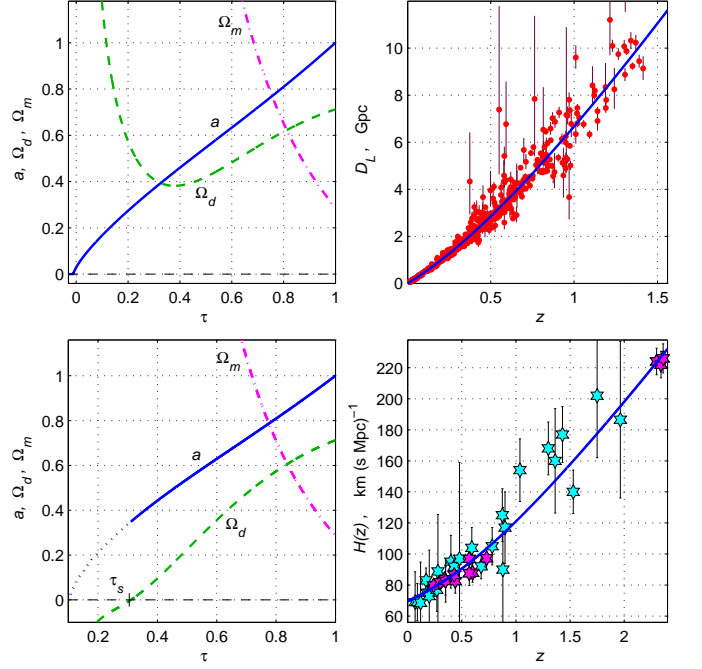


FIG. 2: The figure corresponds to Ansatz I in (19). For the regular solution with optimal parameters from Table III, in the top-left panel we present the graphs of the scale factor $a(\tau)$, densities $\Omega_m(\tau)$, $\Omega_d(\tau)$; and also in the right panels dependencies $D_L(z)$ and $H(z)$ describing SNe data [54] and $H(z)$ data from Table I. In the bottom-left panel we show the example with type (c1) singularity (36) (here $\lambda_m = -0.01$, other parameters are the same).

with the singular solution in the bottom-left panel, whose parameters differ only in one value: $\lambda_m = -0.01$. However, in the last case we have the graphs for the type (c1) singularity (36): the DE density $\Omega_d(\tau) = \rho_d/\rho_{cr}$ (the green dashed line) becomes negative at $\tau < \tau_s$. In these panels we show how the scale factor a (blue solid lines) and densities $\Omega_m = \rho_m/\rho_{cr}$ (magenta dash-dotted lines) and Ω_d depend on the dimensionless time $\tau = H_0 t$.

In the right panels of Fig. 2 we demonstrate how the Ansatz I with parameters from Table III describes SNe data [54] and $H(z)$ data from Table I. The last values are marked as cyan or magenta stars, if they are obtained from differential ages or from BAO data.

We analyze the flat case of Ansatz I (19) in Fig. 3, in particular, χ_Σ^2 , $\chi_{SN}^2 + \chi_{BAO}^2$, $\chi_{SN}^2 + \chi_H^2$ as functions of 2 parameters are studied in 4 bottom panels in notations of Fig. 1. In the top panels we compare this model (blue solid lines) with Ansatz II (20) (brown dash-dotted lines). For these cases optimal values and 1σ estimates of model parameters are calculated separately from one-parameter distributions of $\min \chi_\Sigma^2$ and written in the corresponding lines of Table III.

One should compare Ansatz II (20) ($\beta = 0$) with Ansatz I ($\alpha = 0$), because for these cases we have the same number of model parameters $N_p = 6$. We try to

Variant	$\min \chi^2_\Sigma$	H_0	Ω_k	Ω_{m0}	λ_m	λ_d	EoS parameters
$w_d = \text{const}$	576.29	$70.40^{+2.18}_{-2.13}$	$-0.124^{+0.213}_{-0.190}$	0.285 ± 0.013	$0.115^{+0.217}_{-0.265}$	$-0.093^{+0.230}_{-0.259}$	$w_d = -0.913^{+0.132}_{-0.214}$
$w_d = \text{const}$ & $\Omega_k = 0$	576.64	$69.68^{+1.80}_{-1.75}$	0	0.287 ± 0.013	$0.090^{+0.213}_{-0.260}$	$-0.059^{+0.233}_{-0.280}$	$w_d = -0.994^{+0.123}_{-0.157}$
Ansatz I ($\alpha = 0$)	576.29	$69.55^{+1.80}_{-1.73}$	0	0.288 ± 0.013	$0.173^{+0.09}_{-0.17}$	$-0.277^{+0.407}_{-0.309}$	$w_{d0} = -0.94^{+0.137}_{-0.157}$ $\beta = -0.35^{+0.87}_{-0.44}$
Ansatz II ($\beta = 0$)	576.57	$69.66^{+1.80}_{-1.75}$	0	0.287 ± 0.013	$0.123^{+0.18}_{-0.175}$	$-0.112^{+0.285}_{-0.26}$	$w_{d0} = -0.988^{+0.11}_{-0.135}$ $\alpha = 0.073^{+0.062}_{-0.055}$
Ansatz III ($\alpha = 1$)	576.64	$69.68^{+1.80}_{-1.74}$	0	0.287 ± 0.013	$0.098^{+0.475}_{-0.24}$	$-0.060^{+0.74}_{-0.266}$	$w_{d0} = -0.996^{+0.12}_{-0.155}$ $\beta = 0.997^{+0.243}_{-0.115}$
Ansatz IV Eq. (23)	576.07	$69.23^{+1.90}_{-1.86}$	0	$0.292^{+0.016}_{-0.015}$	$0.237^{+0.076}_{-0.250}$	$-0.452^{+0.73}_{-0.43}$	$w_{d0} = -0.786^{+0.356}_{-0.31}$ $w_1 = -3.14^{+4.30}_{-4.72}$
Ansatz V Eq.(24)	575.97	$69.32^{+1.84}_{-1.74}$	0	0.292 ± 0.015	$0.220^{+0.062}_{-0.245}$	$-0.497^{+0.64}_{-0.386}$	$w_{d0} = -0.810^{+0.338}_{-0.27}$ $w_1 = -2.68^{+3.75}_{-4.03}$

TABLE III: Variants of the model (11) and 1σ estimates of the model parameters from the analysis of SN+H+BAO data.

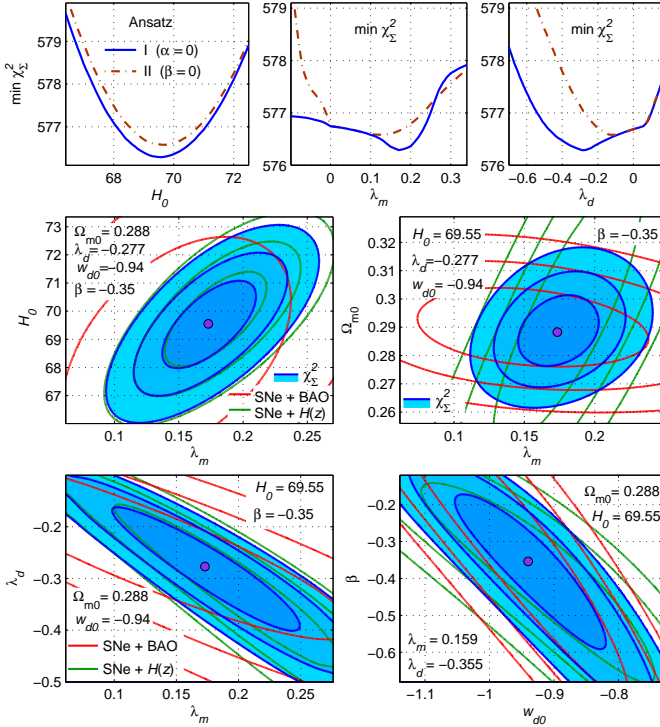


FIG. 3: For Ansatz I in eq. (19) with $\Omega_k = 0$ we present the dependence of $\min \chi^2_\Sigma$ on H_0 , λ_m and λ_d (blue solid lines in the top panels) and level lines in planes of 2 parameters in notations of Fig. 1 (filled contours are for χ^2_Σ). In the top panels we compare this model with Ansatz II under restriction $\Omega_k = 0$ (brown dash-dotted lines).

minimize N_p , hence here and below for all variants of the model we consider only the flat case $\Omega_k = 0$. In comparison in Fig. 3 we see the certain advantage of Ansatz I in absolute minimum of χ^2_Σ , so this variant is presented in

Fig. 3 in detail.

Dependence of $\min \chi^2_\Sigma$ on H_0 in the top-left panel of Fig. 3 is similar for both presented variants of the model. In the middle top panel for these variants we see similar dependence of $\min \chi^2_\Sigma$ on λ_m for $0 < \lambda_m < 0.1$ and different behavior for negative λ_m . The latter fact is connected with different singularities (36) in these variants in the domain $\lambda_m < 0$. Partial coincidence between the variants (19) and (20) can also be seen in the top-right panel, where $\min \chi^2_\Sigma$ depends on λ_d .

The variant (21) (Ansatz III) of our model has the mentioned above advantage: the simple analytic solution (22) for its case $\lambda_m = 0$. However, the best value of $\min \chi^2_\Sigma$, achieved for this variant (see Table III) is worse, than the corresponding minimum for Ansatz I (19), Ansatz IV (23) and for Ansatz V (24). Bad results of Ansatz III (21) are seen in Fig. 4, where this variant is compared with the cases (23) and (24) and with two other cosmological models. One should add that solutions with optimal parameters for Ansatz III are close to singular solutions of types (a) and (c) (36) in the parameter space. In our calculations of values in Table III we had to bypass domains with singular behavior of solutions.

For the case $\lambda_m = 0$ of Ansatz III, considered in Ref. [43], we have the best value $\min \chi^2_\Sigma \simeq 576.81$, so this variant with analytic solutions (22) appeared to be unsuccessful in comparison with the case (13) $w_d = \text{const}$, $\Omega_k = 0$ (for these variants $N_p = 5$, so they are comparable). Due to this reason we do not show in Table III the variant $\lambda_m = 0$, $\alpha = 1$ in a separate line.

The next variant (23) (Ansatz IV) with CPL parametrization [48, 49] behaves better, it has only the type (c1) (36) singularities in the domain $\lambda_m < 0$, but this domain is far from optimal values of the model parameters with the smallest $\min \chi^2_\Sigma \simeq 576.07$ (Table III). In Fig. 4 red dash-dotted lines show, how $\min \chi^2_\Sigma$ depends on H_0 , λ_m and other parameters for the case (23).

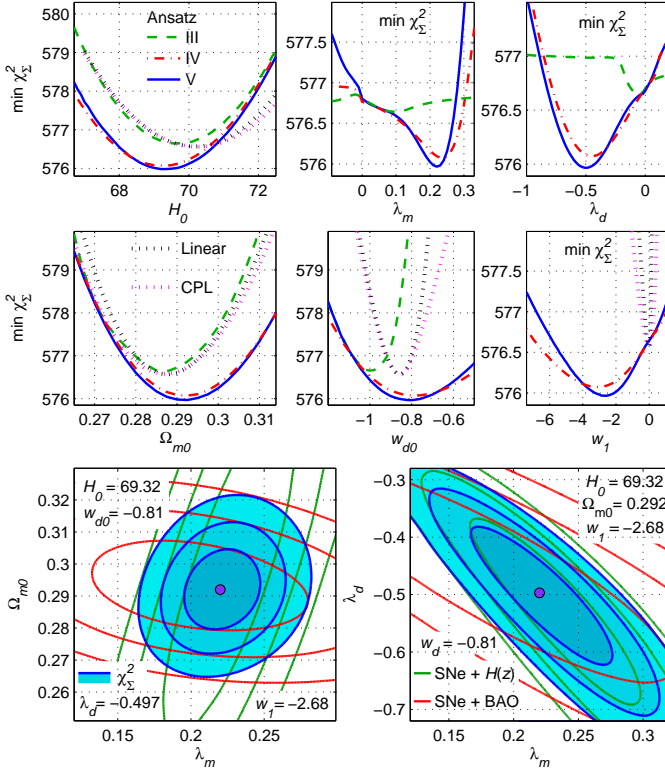


FIG. 4: Dependence of $\min \chi^2_{\Sigma}$ on H_0 , λ_m , λ_d , Ω_{m0} , w_{d0} , w_1 for Ansatz III (21) (green dashed lines), Ansatz IV (23) (red dash-dotted lines) and for Ansatz V (24) (blue solid lines) in comparison with non-interacting models with CPL EoS (40) (magenta dots) and with linear EoS (41) (black dots). Level lines in the bottom panels are shown for Ansatz V in notations of Figs. 1 and 3.

The last variant in Table III (Ansatz V) is the interacting model with linear EoS (24). In this scenario we achieve the absolute minimum among all considered models in Tables III and IV: $\chi^2_{\Sigma} \simeq 575.97$. This value is essentially lower than the result (see in Table IV) for the corresponding model (41) [51–53] without interaction.

In Fig. 4 one can see dependence of $\min \chi^2_{\Sigma}$ on model parameters for Ansatz V (24) (blue solid lines). Their behavior is similar to Ansatz IV (23) (red dash-dotted lines). In the bottom panels for Ansatz V we present level lines for χ^2_{Σ} (filled contours) and also for $\chi^2_{SN} + \chi^2_{BAO}$ (red) and for $\chi^2_{SN} + \chi^2_H$ (green contours).

In the next section we compare our model (11) with other cosmological models. In particular, graphs of $\min \chi^2_{\Sigma}$ for non-interacting models [48, 49, 51–53], corresponding to Ansatz IV (23) and Ansatz V (24) are shown in Fig. 4 with dots.

5. COMPARISON WITH OTHER COSMOLOGICAL MODELS

In this section we compare our interacting dark energy scenario with some other existing cosmological models. In Table IV we demonstrate how these models describe the same observational data for SNe Ia [54], $H(z)$ and BAO from Tables I, II. Calculations were made in accordance with the procedure described in Sect. 4, and in Ref. [84]. Therefore, we will briefly describe the models in the following subsections.

5.1. Modified Chaplygin gas and its family

The equation of state for modified Chaplygin gas (MCG) with pressure p_g and energy density ρ_g is [91, 92]

$$p_g = A\rho_g - \frac{B}{\rho_g^\alpha}. \quad (37)$$

Modified Chaplygin gas is the subsequent generalizations of Chaplygin gas (EoS: $p_g = -B/\rho_g$) and generalized Chaplygin gas (GCG) with EoS [93]:

$$p_g = -B/\rho_g^\alpha. \quad (38)$$

In these models GCG or MCG acts as a unified candidate for dark matter and dark energy.

In Table IV for the MCG and GCG models we cite the results of calculations from Ref. [84], where these scenarios were explored as two-component models with usual dust-like baryonic matter component ρ_b and the Chaplygin gas component ρ_g : $\rho = \rho_b + \rho_g$. In this case the Friedmann equation (3) is

$$H^2/H_0^2 = \Omega_{b0}a^{-3} + \Omega_k a^{-2} + (1 - \Omega_{b0} - \Omega_k) \left[B_s + (1 - B_s) a^{-3(1+A)(1+\alpha)} \right]^{1/(1+\alpha)}.$$

Here the dimensionless parameter $B_s = B\rho_{g0}^{-1-\alpha}/(1+A)$ is used instead of B , and $\rho_{g0} = \rho_g(t_0)$.

For MCG, GCG and other cosmological models the estimations in Table IV were made for the value $\Omega_{b0} = 0.044$ (Eq. (34)). It is shown in Ref. [84], that this value is optimal for the Λ CDM, MCG, GCG and the model with EoS (39), if we use the fitting formula (33). These estimations were supported with the more simple fitting formula $r_d = (r_d h)_{fid} \cdot h^{-1}$, but in the latter case the mentioned models are not sensitive to a value Ω_{b0} in the range $0 \leq \Omega_{b0} \leq 0.15$, because of similarity in properties of dark matter and baryonic matter. Due to this reason we do not consider Ω_{b0} as a free model parameter and fix it in the form (34) for all models in Table IV.

One can see in Table IV that the MCG model demonstrates the value $\min \chi^2_{\Sigma} = 576.45$, it is a bit better than the the $w_d = \text{const}$ model (13). The MCG mode also has $N_p = 5$ parameters: H_0 , Ω_k , A , B_s , α . For the GCG model the minimum of χ^2_{Σ} is worse, however in this case we have $N_p = 4$ parameters (because $A = 0$), so the GCG model gets advantage from information criteria.

5.2. Quadratic equation of state

We consider a cosmic substratum having quadratic equation of state which has similar unified behavior as in MCG. Further, this quadratic EoS asymptotically becomes of de Sitter type. The EoS [84, 94]

$$p = \tilde{p}_0 + w_0 \rho_g + \tilde{\beta} \rho_g^2$$

includes the first three terms of the Taylor series expansion of an arbitrary function $p = f(\rho_g)$, where \tilde{p}_0 , w_0 , $\tilde{\beta}$ are free parameters. It is convenient to rewrite this EoS in the form [84]

$$p = p_0 \rho_c + w_0 \rho_g + \beta \rho_g^2 / \rho_c, \quad (39)$$

where $p_0 = \tilde{p}_0 / \rho_c$, $\beta = \tilde{\beta} \rho_c$ are the dimensionless parameters, $\rho_c = 3H_0^2 / 8\pi G$ is the critical density of the universe.

Solving the conservation equation (5), we obtain the energy density ρ_g in the form

$$\frac{\rho_g}{\rho_c} = \begin{cases} \frac{1}{2\beta} \left[\frac{\Gamma - \sqrt{|\Delta|} \tan\left(\frac{\pi}{2} \sqrt{|\Delta|}\right)}{1 - |\Delta|^{-\frac{1}{2}} \tan\left(\frac{\pi}{2} \sqrt{|\Delta|}\right)} - 1 - w_0 \right], & \Delta < 0, \\ \frac{1}{2\beta} \left[\left(\frac{\pi}{2} + \frac{1}{\Gamma}\right)^{-1} - 1 - w_0 \right], & \Delta = 0, \\ \frac{\rho_- (\Omega_m - \rho_+) a^{-3\sqrt{\Delta}} - \rho_+ (\Omega_m - \rho_-)}{(\Omega_m - \rho_+) a^{-3\sqrt{\Delta}} - \Omega_m + \rho_-}, & \Delta > 0; \end{cases}$$

where $\Delta = (1 + w_0)^2 - 4\beta p_0$, $\Omega_m = 1 - \Omega_k - \Omega_{b0}$, $\Gamma = 2\beta\Omega_m + 1 + w_0$, $\rho_{\pm} = \frac{-1 - w_0 \pm \sqrt{\Delta}}{2\beta}$.

Hence, the evolution equation can be written as

$$H^2 = H_0^2 \left[\frac{\rho_g}{\rho_c} + \Omega_{b0} a^{-3} + \Omega_k a^{-2} \right].$$

The value $\min \chi_{\Sigma}^2 = 576.03$ for the model (39) in Table IV is better than for the MCG model, it is close to the best result of Ansatz V (24).

5.3. CPL parametrization

We also consider the universe including cold dark matter and a dark energy component with Chevallier-Polarski-Linder (CPL) parametrization [48, 49], i.e. Eq. (23)

$$w = w_0 + w_1 \frac{z}{1+z} = w_0 + w_1(1-a), \quad (40)$$

where w_0 , w_1 are two free parameters. In presence of this dark energy component (with its present time fraction $\Omega_{X0} = 1 - \Omega_{m0} - \Omega_k$) the evolution equation is

$$\frac{H^2}{H_0^2} = \Omega_{m0} a^{-3} + \Omega_k a^{-2} + \Omega_{X0} a^{-3(1+w_0+w_1)} e^{3w_1(a-1)}.$$

It is interesting to compare this model with the considered above variant (23) (Ansatz IV) of our interacting

model with the similar EoS. In other words, the CPL model (40) transforms into Ansatz IV (23), if we include the interaction term (11) with two model parameters λ_m , λ_d and fix the curvature parameter $\Omega_k = 0$. We see in Table IV and in Fig. 4 that the interactive scenario (23) (Ansatz IV) has the essential advantage in $\min \chi_{\Sigma}^2 \simeq 576.07$ in comparison with the model (40) ($\min \chi_{\Sigma}^2 \simeq 576.57$).

5.4. Linear parametrization

The model with linear parametrization in EoS is similar to the considered above CPL parametrization (40), but has the following EoS [51–53]

$$w = w_0 + w_1 z, \quad (41)$$

where w_0 , w_1 are two free parameters to be constrained by the observational data. The evolution equation for a universe made of cold matter and the dark energy with the above equation of state is

$$\frac{H^2}{H_0^2} = \Omega_{m0} a^{-3} + \Omega_k a^{-2} + \Omega_{X0} a^{-3(1+w_0-w_1)} e^{3w_1\left(\frac{1-a}{a}\right)}.$$

One can see in Table IV and in Fig. 4 that the model (41) behaves very closely to the CPL scenario (40), but it demonstrates essentially worse $\min \chi_{\Sigma}^2$ than the corresponding interactive model (24) (Ansatz V).

Hierarchy of the scenarios in Table IV will change, if we take into account information criteria which use a number N_p of model parameters (degrees of freedom). In particular, the Akaike information criterion is given by [86–88]

$$AIC = \min \chi_{\Sigma}^2 + 2N_p.$$

This criterion gives advantage to the Λ CDM and other models with minimal N_p .

6. SUMMARY

In the FLRW background of our universe we have considered an interacting scenario between dark matter and dark energy where both of them are barotropic in nature. The interaction is a linear combination of the energy densities of the dark components in the form $Q = 3H\lambda_m\rho_m + 3H\lambda_d\rho_d$, where (λ_m, λ_d) are the coupling parameters describing the strength and direction of energy flow (i.e. whether $Q > 0$ or $Q < 0$) from their sign. Since the EoS in DE could be either constant or variable in nature, hence we have examined both the possibilities to explore the cosmological scenarios with the use of current astronomical data. For $w_d = \text{constant}$ the evolution equations for matter and dark energy take analytic forms, which is one of the important findings in the current work, because for most of the interactions, the

Model	$\min \chi^2_\Sigma$	H_0	other parameters	N_p	AIC
$w_d = \text{const}$ (non-flat)	576.29	$70.4^{+2.18}_{-2.13}$	$\Omega_k = -0.124, \Omega_{m0} = 0.285, \lambda_m = 0.115, \lambda_d = -0.093, w_d = -0.913$	6	588.29
$w_d = \text{const}$ (flat)	576.64	$69.68^{+1.80}_{-1.75}$	$\Omega_k = 0, \Omega_{m0} = 0.287, \lambda_m = 0.09, \lambda_d = -0.059, w_d = -0.994$	5	586.64
Ansatz I [Eq. (19)]	576.29	$69.55^{+1.80}_{-1.73}$	$\Omega_{m0} = 0.288, \lambda_m = 0.173, \lambda_d = -0.277, w_{d0} = -0.94, \beta = -0.35$	6	588.29
Ansatz IV [Eq. (23)]	576.07	$69.23^{+1.90}_{-1.86}$	$\Omega_{m0} = 0.292, \lambda_m = 0.237, \lambda_d = -0.452, w_{d0} = -0.786, w_1 = -3.14$	6	588.07
Ansatz V [Eq. (24)]	575.97	$69.32^{+1.84}_{-1.74}$	$\Omega_{m0} = 0.292, \lambda_m = 0.220, \lambda_d = -0.497, w_{d0} = -0.81, w_1 = -2.68$	6	587.97
ΛCDM	578.56	$69.32^{+1.81}_{-1.79}$	$\Omega_{m0} = 0.278 \pm 0.009, \Omega_\Lambda = 0.753^{+0.050}_{-0.057}, \Omega_k = -0.027 \pm 0.049$	3	584.56
GCG [Eq. (38)]	577.01	69.59 ± 1.90	$\alpha = -0.112 \pm 0.097, B_s = 0.737 \pm 0.024, \Omega_k = 0.029 \pm 0.074$	4	585.01
MCG [Eq. (37)]	576.45	70.35 ± 2.15	$\alpha = 0.540^{+0.90}_{-0.895}, B_s = 0.711^{+0.034}_{-0.031}, \Omega_k = -0.041^{+0.125}_{-0.12},$ $A = -0.168^{+0.323}_{-0.090}$	5	586.45
Quadratic EoS [Eq. (39)]	576.03	$70.40^{+2.06}_{-2.03}$	$p_0 = -0.895^{+0.215}_{-0.23}, \beta = -0.045^{+0.038}_{-0.036}, \Omega_k = -0.044 \pm 0.065,$ $w_0 = 0.194^{+0.205}_{-0.190}$	5	586.03
CPL [Eq. (40)]	576.57	$70.22^{+2.15}_{-2.07}$	$\Omega_{m0} = 0.287^{+0.014}_{-0.013}, \Omega_k = -0.16^{+0.147}_{-0.165}, w_0 = -0.857^{+0.105}_{-0.103},$ $w_1 = -0.02^{+0.42}_{-0.82}$	5	586.57
Linear [Eq. (41)]	576.57	$70.18^{+2.08}_{-2.03}$	$\Omega_{m0} = 0.288^{+0.013}_{-0.012}, \Omega_k = -0.149^{+0.143}_{-0.173}, w_0 = -0.856^{+0.082}_{-0.10},$ $w_1 = -0.022^{+0.16}_{-0.474}$	5	586.57

TABLE IV: Comparison of several cosmological models has been presented.

background can not be analytically solved. For variable w_d we have proposed three ansatze in Eqns. (19), (20), (21), which emerge from the generalized ansatz given in Eq. (17). In addition to these, we have considered two more variable EoS in DE in the forms of CPL and linear parametrizations in equations (23), (24), respectively. Altogether, we have considered 7 variants for the present interacting model for a detailed analysis.

Henceforth, with the introduction of 7 variants of the EoS in dark energy, we constrained the model parameters by the joint analysis of recent 580 Union 2.1 data points, 39 Hubble parameter data points, and 17 baryon acoustic oscillation data points using of statistical minimization technique and presented the results in Table III.

We found that for $w_d = \text{constant}$, the curvature parameter Ω_k plays significant role in the analysis. We investigated the cases $\Omega_k \neq 0$ and $\Omega_k = 0$, the difference in behavior of $\min \chi^2_\Sigma$ for them has been presented in the top panels of Fig. 1 and in Table III. For the case $\Omega_k \neq 0$ of the model with $w_d = \text{constant}$, the minimal value of χ^2_Σ is better, so for this case we presented two dimensional contour plots at $1\sigma, 2\sigma, 3\sigma$ confidence levels in Fig. 1.

Further, the possibility of variable EoS in DE has been investigated with 5 different variants in Eqs. (19) – (24) for the present interaction. We found that the variants may experience singularities (see Fig. 2) at finite time, and hence, we excluded the domains of the parameters leading to the singular behavior and analyzed them by the current data sets mentioned above. In most of the cases we notice that one of the coupling parameters of the interaction possesses negative sign, which hints that during the evolution of the universe the present interaction Q could change its sign, thereby the direction of energy flow may change.

In figures 3, 4, we have presented the graphical nature of the $\min \chi^2_\Sigma$ over the model parameters for the variable EoS in DE presented in the paper. For Ansatz I and Ansatz V (linear parametrization), we have presented the contour plots in the two dimensional plane for several couple of model parameters at $1\sigma, 2\sigma, 3\sigma$ confidence levels.

Finally, the interaction model with some variants, such as, $w_d = \text{constant}$, Ansatz I, Ansatz IV, Ansatz V have been compared and constrained by the same data sets with some known cosmological models, such as, ΛCDM model, unified models, namely, the generalized Chaplygin gas (GCG), modified Chaplygin gas (MCG), a fluid with quadratic equation of state, and finally with CPL and linear parametrizations in DE. The results have been presented in Table IV.

It is found that the present interacting DE model with constant w_d slightly favors the phantom region in agreement with the latest report [42]. The best absolute value of $\min \chi^2_\Sigma$ is achieved for the interacting model with EoS (24) (Ansatz V). The second result demonstrates that among the non-interacting models the model with quadratic EoS in (39) provides a better fit with the observational data. However, the number of model parameters of this non-interacting model ($N_p = 5$) is less than the number of model parameters for the interacting model (24), but larger than the number of model parameters in models GCG or ΛCDM .

Finally, we notice that although different models have different model parameters, still from AIC analysis, the models presented in Table IV do not deviate so much from the ΛCDM model with minimum number of model parameters in comparison with others.

ACKNOWLEDGMENTS

SP was supported by the Science and Engineering Research Board through NPDF (File No:

PDF/2015/000640). G.S.S was supported by the Ministry of education and science of Russia, grant No. 1686.

-
- [1] A. G. Riess *et al.*, *Astron. J.*, **116**, 1009 (1998).
[2] S. Perlmutter *et al.*, *Astrophys. J.*, **517**, 565 (1999).
[3] W.J. Percival *et al.*, *Mon. Not. R. Astron. Soc.* **327**, 1297 (2001).
[4] D.N. Spergel *et al.*, *Astrophys. J. Suppl.* **148**, 175 (2003).
[5] M. Tegmark *et al.*, *Phys. Rev. D* **69**, 103501 (2004).
[6] D.J. Eisenstein *et al.*, *Astrophys. J.* **633**, 560 (2005).
[7] E. Komatsu *et al.*, *Astrophys. J. Suppl.* **192**, 18 (2011).
[8] S. Weinberg, *Rev. Mod. Phys.* **61**, 1 (1989).
[9] P. J. Steinhardt, *Phil. Trans. Roy. Soc. Lond. A.*, **361**, 2497 (2003).
[10] L. Amendola and S. Tsujikawa, *Dark Energy: Theory and Observations*, Cambridge University Press, Cambridge UK (2010).
[11] Planck Collaboration, *Astron. Astrophys.* **571**, A16 (2014).
[12] Planck Collaboration, “Planck 2015 results. XIII. Cosmological parameters”, arXiv:1502.01589 [astro-ph.CO].
[13] A. Rest *et al.*, *Astrophys. J.* **795**, 44 (2014).
[14] C. Cheng, and Q.-G Huang, *Phys. Rev. D* **89**, 043003 (2014).
[15] D.L. Shafer and D. Huterer, *Phys. Rev. D* **89**, 063510 (2014).
[16] R.R. Caldwell, *Phys. Lett. B* **545**, 23 (2002).
[17] S.M. Carroll, M. Hoffman and M. Trodden, *Phys. Rev. D* **68**, 023509 (2003).
[18] J.M. Cline, S. Jeon and G. D. Moore, *Phys. Rev. D* **70**, 043543 (2004).
[19] S.D.H. Hsu, A. Jenkins, and M.B. Wise, *Phys. Lett. B* **597**, 270 (2004).
[20] F. Sbisà, *Eur. J. Phys.* **36**, 015009 (2015).
[21] M. Dabrowski, *Eur. J. Phys.* **36**, 065017 (2015).
[22] C. Wetterich, *Astron. Astrophys.* **301**, 321 (1995).
[23] L. Amendola, *Phys. Rev. D* **62**, 043511 (2000).
[24] A. P. Billyard and A. A. Coley, *Phys. Rev. D* **61**, 083503 (2000).
[25] W. Zimdahl, D. Pavon, and L. P. Chimento, *Phys. Lett. B* **521**, 133 (2001).
[26] L. Amendola and C. Quercellini, *Phys. Rev. D* **68**, 023514 (2003).
[27] R. Herrera, D. Pavon, and Winfried Zimdahl, *Gen. Rel. Grav.* **36**, 2161 (2004).
[28] L. P. Chimento, A. S. Jakubi, D. Pavon, and W. Zimdahl, *Phys. Rev. D* **67**, 083513 (2003).
[29] J.-H. He and B. Wang, *J. Cosmol. Astropart. Phys.* **0806**, 010 (2008).
[30] M. Quartin *et al.*, *J. Cosmol. Astropart. Phys.* **0805**, 007 (2008).
[31] C. G. Boehmer, G. Caldera-Cabral, R. Lazkoz, and R. Maartens, *Phys. Rev. D* **78**, 023505 (2008).
[32] G. Caldera-Cabral, R. Maartens, and L. A. Urena-Lopez, *Phys. Rev. D* **79**, 063518 (2009).
[33] L. P. Chimento, *Phys. Rev. D* **81**, 043525 (2010).
[34] R. C. Nunes and E. M. Barboza, *Gen. Rel. Grav.* **46**, 1820 (2014), arXiv:1404.1620 [astro-ph.CO].
[35] J. Sola, J. d. C. Perez, A. Gomez-Valent and R. C. Nunes, arXiv:1606.00450 [gr-qc].
[36] Yu. L. Bolotin, A. Kostenko, O.A. Lemets, and D.A. Yerokhin, *Int. J. Mod. Phys. D* **24**, 1530007 (2014).
[37] B. Wang, E. Abdalla, F. Atrio-Barandela and D. Pavon, arXiv:1603.08299 [astro-ph.CO].
[38] W. Zimdahl, *Int. J. Mod. Phys. D.*, **14**, 2319 (2005).
[39] B. Wang, J. Zang, C. -Y. Lin, E. Abdalla, and S. Micheletti, *Nucl. Phys. B.*, **778**, 69 (2007).
[40] H. Mohseni Sadjadi and M. Honardoost, *Phys. Lett. B* **647**, 231 (2007).
[41] S. Pan and S. Chakraborty, *Int. J. Mod. Phys. D* **23**, 1450092 (2014).
[42] R. C. Nunes, S. Pan and E. N. Saridakis, *Phys. Rev. D* **94**, 023508 (2016).
[43] S. Pan, S. Bhattacharya, and S. Chakraborty, *Mon. Not. R. Astron. Soc.* **452**, 3038 (2015).
[44] A. Paliathanasis and M. Tsamparlis, *Phys. Rev. D* **90**, no. 4, 043529 (2014).
[45] J. L. Tonry *et al.*, *Astrophys. J.* **594**, 1 (2003) (arXiv: astro-ph/0305008).
[46] B. J. Barris *et al.*, *Astrophys. J.* **602**, 571 (2004) (arXiv: astro-ph/0310843).
[47] J. S. Wang and F.Y. Wang, *Astron. Astrophys.* **564**, A137 (2014).
[48] M. Chevallier and D. Polarski, *Int. J. Mod. Phys. D* **10**, 213 (2001).
[49] E. V. Linder, *Phys. Rev. Lett.* **90**, 091301 (2003).
[50] A. G. Riess, *et al.*, *Astrophys. J.* **659**, 98, (2007).
[51] P. Astier, *Phys. Lett. B* **500**, 8 (2001).
[52] A. R. Cooray and D. Huterer, *Astrophys. J.* **513**, L95 (1999).
[53] J. Weller and A. Albrecht, *Phys. Rev. D* **65**, 103512 (2002).
[54] N. Suzuki *et al.*, *Astrophys. J.* **746**, 85 (2012).
[55] J. Simon, L. Verde and R. Jimenez, *Phys. Rev. D* **71**, 123001 (2005).
[56] D. Stern, R. Jimenez, L. Verde, M. Kamionkowski and S. A. Stanford, *J. Cosmol. Astropart. Phys.* **1002**, 008 (2010).
[57] M. Moresco *et al.*, *J. Cosmol. Astropart. Phys.* **1208**, 006 (2012).
[58] C. Zhang *et al.*, *Res. Astron. Astrophys.* **14**, 1221 (2014).
[59] M. Moresco, *Mon. Not. Roy. Astron. Soc.*, **450** L16 (2015).
[60] M. Moresco *et al.*, arXiv:1601.01701 [astro-ph.CO].
[61] E. Gaztañaga, A. Cabre, L. Hui, *Mon. Not. Roy. Astron. Soc.* **399**, 1663 (2009).
[62] C. Blake *et al.*, *Mon. Not. Roy. Astron. Soc.* **425**, 405 (2012).
[63] N. G. Busca *et al.*, *Astron. Astrophys.* **552**, A96 (2013).
[64] C-H. Chuang and Y. Wang, *Mon. Not. Roy. Astron. Soc.* **435**, 255 (2013).
[65] C-H. Chuang *et al.*, *Mon. Not. Roy. Astron. Soc.* **433**, 3559 (2013).

- [66] L. Anderson *et al.*, *Mon. Not. Roy. Astron. Soc.* **439**, 83 (2014).
- [67] L. Anderson *et al.*, *Mon. Not. Roy. Astron. Soc.* **441**, 24 (2014).
- [68] A. Oka *et al.*, *Mon. Not. Roy. Astron. Soc.* **439**, 2515 (2014).
- [69] A. Font-Ribera *et al.*, *J. Cosmol. Astropart. Phys.* **1405**, 027 (2014).
- [70] T. Delubac *et al.*, *Astron. Astrophys.* **574**, A59 (2015).
- [71] W. J. Percival *et al.*, *Mon. Not. Roy. Astron. Soc.* **401**, 2148 (2010).
- [72] E. A. Kazin *et al.*, *Astrophys. J.* **710**, 1444 (2010).
- [73] F. Beutler *et al.*, *Mon. Not. Roy. Astron. Soc.* **416**, 3017 (2011).
- [74] C. Blake *et al.*, *Mon. Not. Roy. Astron. Soc.* **418**, 1707 (2011).
- [75] N. Padmanabhan *et al.*, *Mon. Not. Roy. Astron. Soc.* **427**, 2132 (2012).
- [76] H.-J. Seo *et al.*, *Astrophys. J.* **761**, 13 (2012).
- [77] E. A. Kazin *et al.*, *Mon. Not. Roy. Astron. Soc.* **441**, 3524 (2014).
- [78] A. J. Ross *et al.*, *Mon. Not. Roy. Astron. Soc.* **449**, 835 (2015).
- [79] G. Hinshaw *et al.*, *Astrophys. J. Suppl. Ser.* **208**, 19 (2013).
- [80] S. Nesseris and L. Perivolaropoulos, *Phys. Rev. D* **72**, 123519 (2005).
- [81] A. Conley *et al.*, *Astrophys. J. Suppl. Ser.* **192**, 1 (2011).
- [82] E.J. Ruiz, D.L. Shafer, D. Huterer, and A Conley, *Phys. Rev. D* **86**, 103004 (2012).
- [83] E. Aubourg *et al.*, *Phys. Rev. D* **92**, 123516 (2015).
- [84] G. S. Sharov, *J. Cosmol. Astropart. Phys.* **06**, 023 (2016).
- [85] K. Bamba, S. Capozziello, S. Nojiri, and S. D. Odintsov, *Astrophys. Sp. Sc* **342**, 155 (2012).
- [86] H. Akaike, *IEEE Transactions of Automatic Control* **19**, 716 (1974).
- [87] M. Szydlowski, A. Kurek, and A. Krawiec, *Phys. Lett. B* **642**, 171 (2006).
- [88] K. Shi, Y. F. Huang, and T. Lu, *Mon. Not. Roy. Astron. Soc.* **426** (2012) 2452.
- [89] J.-H. He, B. Wang, and E. Abdalla, *Phys. Lett. B* **671**, 139 (2008).
- [90] J. Valiviita, E. Majerotto, and R. Maartens, *J. Cosmol. Astropart. Phys.* **0807**, 020 (2008).
- [91] U. Debnath, A. Banerjee, and S. Chakraborty, *Class. Quant. Grav.* **21**, 5609 (2004).
- [92] H. B. Benaoum, arXiv:hep-th/0205140.
- [93] A. Y. Kamenshchik, U. Moschella and V. Pasquier, *Phys. Lett. B* **511**, 265 (2001).
- [94] K. N. Ananda and Marco Bruni, *Phys. Rev. D* **74**, 023523 (2006).